Available online at www.sciencedirect.com
ScienceDirect
Journal of the European Ceramic Society 30 (2010) 1089–1096
www.elsevier.com/locate/jeurceramsoc

Impedance study of the electrophoretic deposition of yttrium silicate from a polymeric precursor sol

Oliver Schneider [a,*], Jana Große-Brauckmann [a], Christos Argirusis [a,b]

[a] *Institut für Metallurgie, Technische Universität Clausthal, D-38678 Clausthal-Zellerfeld, Germany*
[b] *School of Chemical Engineering, National Technical University of Athens, Iroon Polytechneiou 9, Zografou 15780, Athens, Greece*

Available online 9 August 2009

Abstract

A polymeric yttrium silicate sol was prepared for the electrophoretic deposition of Y_2SiO_5 on C/C composite materials. The properties of the sol and the process of electrophoretic deposition (EPD) from the sol on glassy carbon substrates were studied using impedance spectroscopy. During constant voltage electrophoretic deposition first a rapid and thereafter a more gradual decay in current was observed, accompanied by the formation of a thin layer of an Y_2SiO_5 green body. Impedance spectroscopy after the end of the EPD experiment revealed that the resistance of the green body did not significantly increase the impedance of the EPD setup. The impedance spectra measured after EPD changed rapidly with time within the first few minutes, showing a decrease in the resistance of the green body and an increasing charge transfer resistance at the electrodes. This behavior could be related to the formation of a reaction product of electrochemical processes taking place during EPD, and points to ion depletion in the deposit layer.

Keywords: A. Sol–gel processes; C. Electrical conductivity; Electrophoretic deposition; Impedance; D. Y_2SiO_5

1. Introduction

Their outstanding mechanical properties and high strength make C/C composites an attractive structural material for high temperature applications.[1] The major advantage is their excellent thermal shock behavior combined with a relatively low density. Likewise, the materials have great potential in harsh terrestrial temperature environments. One serious drawback is their poor oxidation resistance.[2,3] To take advantage of these materials' benefits a suitable protection against oxidation is needed. For this purpose SiC layers are employed which are usually deposited by means of chemical vapour deposition and allow temperatures of up to 1300 °C.[4] For higher temperatures the coating must be complemented by an outer oxygen diffusion barrier coating.

Yttrium silicate with its high melting point, low oxygen permeation and a thermal expansion coefficient similar to SiC is a promising material for such an outer barrier coating.[5,6] Various coating procedures have been applied to create protective coatings on the C/C–Si–SiC composites such as slip casting,[7] plasma spray[8] and electrophoretic deposition.[9,10]

Electrophoretic deposition (EPD) in this context favours high packing densities and easy control over the deposit thickness. In this technique usually powder particles are dispersed in a solvent where they acquire a certain charge. Under the influence of an electric field these charged particles will move to the oppositely charged electrode where they will be deposited.

Sol–gel synthesis provides an elegant method to directly prepare such a colloidal system of ultrapure nano-sized homogeneously dispersed particles. Therefore the preparation of suitable sol–gel systems for EPD is of great interest. EPD from particulate sols of mullite[11] or silica[12] as well as from polymeric precursor sols[13] are reported in literature.

EPD processes have found numerous applications for the inexpensive and controlled preparation of coatings and ceramic materials, and therefore are of high technological importance. Several reviews have been published.[14–18] Despite a number of papers discussing kinetics and mechanism of EPD processes[14,16,19–24] there is still a lack of understanding regarding the detailed mechanisms involved. This especially concerns

* Corresponding author. Tel.: +49 5323723186; fax: +49 5323723184.
E-mail address: oliver.schneider@tu-clausthal.de (O. Schneider).

0955-2219/$ – see front matter © 2009 Elsevier Ltd. All rights reserved.
doi:10.1016/j.jeurceramsoc.2009.07.020

the microscopic processes taking place during formation of the green layer. Even though EPD is not a faradaic process the current flowing through the suspension has to cross the interface between suspension and substrate. Therefore electrochemical processes must be taking place at this interface. Such reactions are only occasionally discussed in literature.[20,22,23,25] Charge carriers must be transported through the deposited layer to the substrate surface. Depending on the deposition conditions such transport processes can then control the further growth of the layers.[21,26,27] This can be one of the causes for the typical decay in electrical current during constant voltage EPD. Other contributions to this behavior can arise from a large resistance of the as-deposited layer,[19,21,28] a depletion of suspended particles,[21] a change in local field strength,[19,29] ionic depletion,[22,23,25] and ion-selectivity of the green layer by overlapping of diffuse double layers of the particles in the deposit across the pores.[24] An elegant way to study the effect of a deposited layer and to determine some of the relevant electrical properties of a suspension or sol for EPD is impedance spectroscopy (IS).[22,26,30] In IS, one applies (or superimposes to a DC voltage) a small sinusoidal alternating voltage, and measures the resulting alternating current.[31,32] The obtained dependence of the complex impedance on the angular frequency ω allows the extraction of parameters like conductivities, dielectric constants, electrochemical reaction rates, double layer capacitances, diffusion constants, and others. It is a standard technique in electrochemistry[31,32], but rarely applied for the analysis of EPD processes.[22,26,30] The aim of this work therefore was to apply this method to study the EPD of yttrium silicate green bodies from a polymeric precursor sol.

2. Experimental

The yttrium silicate sol was prepared from tetraethoxysilane (TEOS, $Si(OC_2H_5)_4$, Merck for synthesis) and yttriumoxoisopropoxide (YPr, $Y_5O(OC_3H_7)_{13}$, Strem Chemicals, 98%+). Dry isopropanol (IPr, Fluka, $c(H_2O) < 0.005\%$) was used as solvent.

In order to adjust the reaction rates separate 0.1 M solutions of the two alkoxides were prepared. The one containing TEOS was pre-hydrolyzed for 2 days with water of pH 2 and a water to alkoxide ratio (r_W) of 10. Yttriumoxoisopropoxide was dissolved and stabilized in isopropanol using concentrated nitric acid (HNO_3-65%, Merck, Suprapur) and acetyl acetone (AcAc, Merck, for analysis) under argon atmosphere in a glove-box. For 1 mol Y^{3+} cations, 2.65 mol HNO_3 and 1 mol AcAc were added. The as prepared sols were diluted to a concentration of 0.025 mol/l and mixed corresponding to the Y/Si ratio in Y_2SiO_5. A polymeric clear yellowish sol resulted. To increase the electrophoretic mobility of the sol species, 0.25 M KOH was added to the sol by means of a titrator. The resultant sol composition was: YPr:TEOS:HNO_3:KOH:IPr:H_2O = 2:1:5.3:1:1620:34.23.

Electrophoretic mobility and conductivity of the sol were measured in a folded capillary cell using a Zetasizer NanoZS (Malvern, UK).

EPD experiments were carried out using a home-built setup described elsewhere.[13] For the sol characterization two partially immersed glass slides sputter-coated with gold on one side were used. Contact with the cables was made on the non-immersed parts. The immersed electrode area was $A_{im} = 4.8\ cm^2$, the area in air $A_{air} = 3.5\ cm^2$. During the EPD experiments, these electrodes were shortened and used as counter electrodes. Polished plates of glassy carbon (GC, 1 mm × 10 mm × 10 mm) were used as substrate and therefore as working electrode. The distance d between the electrodes was controlled by means of micrometer screws and fixed to 10 mm (between GC substrate and each Au electrode) for the deposition experiments.

Deposition was performed by applying a voltage supplied by a Lambda Genesys power supply between substrate and counter electrodes. The glassy carbon substrate was connected to the negative pole and current transients were recorded during deposition experiments.

Impedance measurements were carried out at open circuit potential in the two electrode configuration using a Zahner Electric IM6 impedance spectrum analyzer. The amplitude of the AC voltage was set to 10 mV (100 mV for measurements in air), and the frequency f varied between 500 mHz (100 mHz for deposition studies) and 100 kHz, except if noted otherwise. For each frequency the ac current was measured for several cycles in order to increase accuracy. For the measurements in sol without deposition, one of the Au electrodes was connected to the working electrode (WE) cable of the IM6, and the other one to counter (CE) and reference electrode (RE) cables. The distance d between the electrodes was varied in 2 mm increments between 1.3 and 2.9 cm. For the measurements after EPD experiments, the substrate was connected to the WE cable, and both gold electrodes (shortened) to CE and RE cables. A measurement in parallel to EPD as in the work of Stappers et al. was not possible with the equipment.[22] After selected EPD experiments a time series was performed, where within 10 min impedance spectra were recorded quickly one after the other in a limited frequency range.

3. Results

3.1. Characterization of the sol

The sol was characterized by measuring the electrophoretic mobility μ and specific conductivity σ in the Zetasizer. The results obtained were $\mu = 1.2 \times 10^{-5}\ cm^2\ V^{-1}\ s^{-1}$ and $\sigma = 1.7 \times 10^{-5}\ S\ cm^{-1}$. In addition impedance measurements between two partially immersed gold-coated glass slides with varying distance d were performed in the same cell used subsequently for EPD. The resulting spectra are shown in Fig. 1 in the complex plane plot, where the imaginary part of the impedance Im(Z) is plotted as a function of its real part Re(Z). Each spectrum showed a portion of a semicircular arc at high frequencies. At intermediate frequencies, Im(Z) decreased to ~0 Ω. At even lower frequencies the spectrum has the shape of a tilted line, i.e. Im(Z) increased linearly with Re(Z). A stepwise increase in distance from d = 1.3 cm to d = 2.9 cm caused a shift of the spectra to higher Re(Z)-values, and a more pronounced linear region of the spectra. Re(Z) at Im(Z) = 0 Ω increases from 12.8 to 20.3 kΩ. Impedance data measured between a GC electrode centered

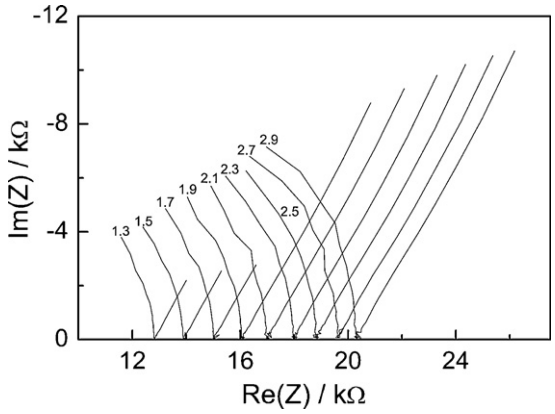

Fig. 1. Impedance spectra measured in a polymeric yttrium silicate sol at electrode distances d between 1.3 and 2.9 cm. For each spectrum the exact value of d is given in the figure ([d] = cm).

between the two Au electrodes, and the shortened Au electrodes prior to any electrophoretic deposition sometimes showed another semicircle at low frequencies rather than a straight line, and sometimes there was also a (partial) semicircle followed by a straight line.

Impedance measurements with the same setup were also performed in air at $d = 1.58$ cm (10^5 to 10^3 Hz) and at distances between $d = 1.58$ cm and $d = 2.5$ cm in 0.5 M NaCl. This was done in order to check for contributions of the experimental setup, especially the resistance of the gold layers on the glass slides, to the overall impedance. From the measurements in air a capacitance of 3.4×10^{-11} F was obtained, which is much larger than expected for the geometric capacitance of two gold electrodes alone. The measurements in NaCl showed Re(Z) values of around 6 Ω at high frequencies.

3.2. Electrophoretic deposition

Electrophoretic deposition was performed from the sol on glassy carbon substrates at voltages of 100 and 200 V for different deposition times. In some experiments, deposition was performed stepwise in order to measure impedance as a function of deposition time. Fig. 2 shows typical current transients obtained during stepwise and one-step depositions. The reproducibility of the measurements was not always as good as in Fig. 2, probably caused by minor asymmetries in the electrode setup. On bare substrates, the current initially decayed rapidly. This period can be satisfactorily described by an exponential decay. After a few seconds, the current decreased more slowly. At longer times, the current decayed with $d^2I/dt^2 > 0$, and was closer to a dependence of I on $t^{-0.5}$.

During one-step experiments, the current decayed throughout the deposition. In the example shown in Fig. 2 the current dropped within 4.5 min to roughly one-third of its original value. If one interrupted the deposition, however, for a few minutes, the current in the next deposition step was much larger than during continuous deposition. The initial currents scaled roughly with the deposition voltage. In terms of ohmic resistances, they corresponded to values of 11–12 kΩ. After a few minutes,

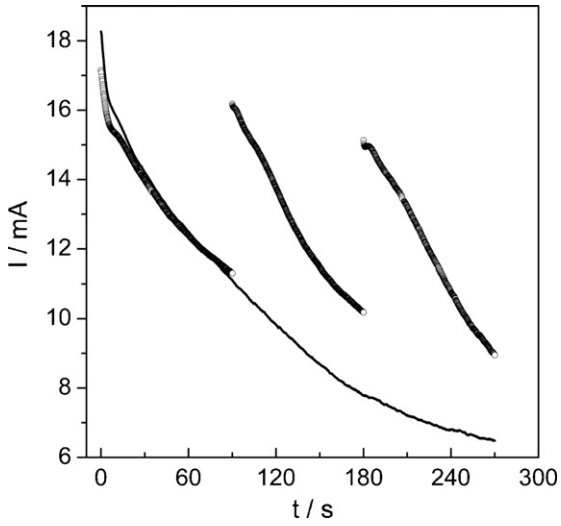

Fig. 2. Current transients measured during stepwise EPD (circles, 90 s deposition time each) and one-step deposition (line, 270 s) at a deposition voltage of 200 V between Au counter electrodes and GC substrate.

the difference in currents became less than expected from the voltages applied. Typically, the currents after 4 min ($R = U/I$) corresponded to numbers between 22 and 32 kΩ.

The mass of the green layers formed after deposition with a deposition charge of $0.7C$–$3C$ varied between 0.4 and 2.4 mg. For deposition times shorter than 60 s no deposit was observed. The composition of the deposits was checked after drying by EDX. Measurements on different substrates revealed a Y:Si atomic ratio of 2:1, as expected from the composition of the sol.

The impedance spectra measured between the GC substrate and the Au counter electrodes was similar to the one measured between the Au electrodes (*cf.* Fig. 3). However, in some cases instead of a line rather a second semicircle was seen at low frequencies. In the high frequency region the shape of the spectra

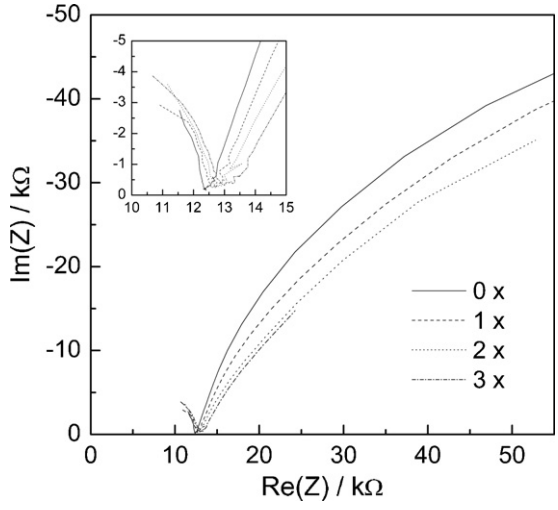

Fig. 3. Impedance spectra measured between GC substrate and Au counter electrodes before (0×) and after three consecutive deposition steps (120 s, 100 V each). The IS spectra were recorded ~730 s (first step) and ~650 s (second and third step) after the respective deposition step.

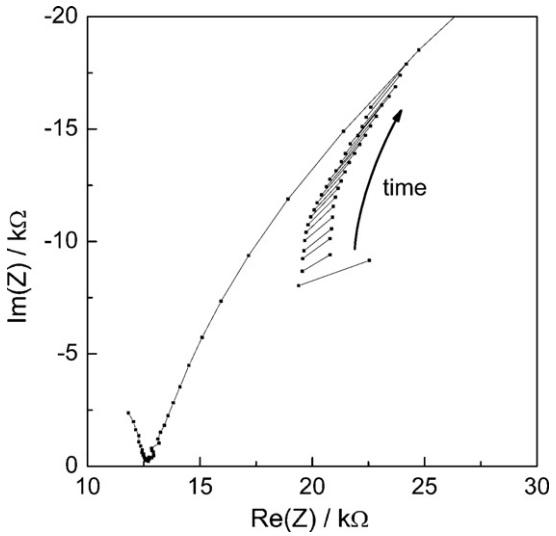

Fig. 4. Time series of impedance data recorded at frequencies of 0.5 and 0.6 Hz, and full impedance spectrum measured after the end of the time series. Data were recorded after one deposition step (120 s, 100 V) on a GC substrate and recording started at times of 207, 246, 268, 291, 313, 334, 356, 378, 400, 422, 443, 465, 487, 509, 531, 553, 575, 597.5, 619.6, 642, 664 and 730 s after the end of the deposition.

was not strongly altered after the individual deposition steps. Only a slight increase of the intercept of the high frequency arc with the abscissa was seen, amounting to about 600 Ω for the example shown in Fig. 3(insert). The diameter of the low frequency semicircle decreased during subsequent deposition steps. However, it was found that the diameter of the low frequency semicircle depended significantly on the time passed between the end of the deposition experiment and the impedance measurement. In general it was very small immediately after deposition, and thereafter increased with time. Therefore the observed impedance decrease with thickness might be in truth a time effect. In order to study this behavior more closely, a series impedance experiment was performed immediately after the end of a deposition step at only two frequencies located well in the low frequency semicircle (Fig. 4).

Both real and imaginary part of the impedance increased with time in magnitude but the changes in Im(Z) were larger. Sometimes in the beginning of the measurements the slope of the curves was even negative, indicating a position on the right side of the semicircle. In the complex plane plot the data recorded in a limited frequency range approached gradually the curve of the full impedance spectrum measured after the end of the time series. In order to study if also the high frequency arc shows some dependency on time after deposition, analogous experiments were performed in the high frequency region (20–1 kHz). These experiments indeed show a small shift of the curves and of the intercept with the abscissa to lower values of Re(Z).

4. Discussion

4.1. Equivalent circuits

The complete equivalent circuit (EC) to describe the impedance response between the two gold electrodes or between a GC electrode and the Au counter electrodes in order to characterize the sol and the EPD process is shown in Fig. 5a. Besides the resistance of cables and the Au electrodes R_{cab} it contains the geometric capacitances $C_{g,air}$, describing the capacitance between the non-immersed parts of the Au-coated glass slides and parasitic capacitances associated with the entire measurement setup, and $C_{g,sol}$, the contribution of the immersed parts. The latter is determined by the dielectric constant of the sol. From a single impedance spectrum only the sum of these two capacitances can be determined. The ohmic resistivity of the precursor sol R_{sol} is electrically connected in parallel with the geometric capacitances. The resistance of an electrophoretically formed deposit layer R_{lay} is connected serially with R_{sol}. The same is true for the interfacial impedance associated with electrochemical reactions taking place at the surface of the electrodes and their double layer capacitance. It consists of two parallel branches, one containing the charge transfer resistance R_{ct} in

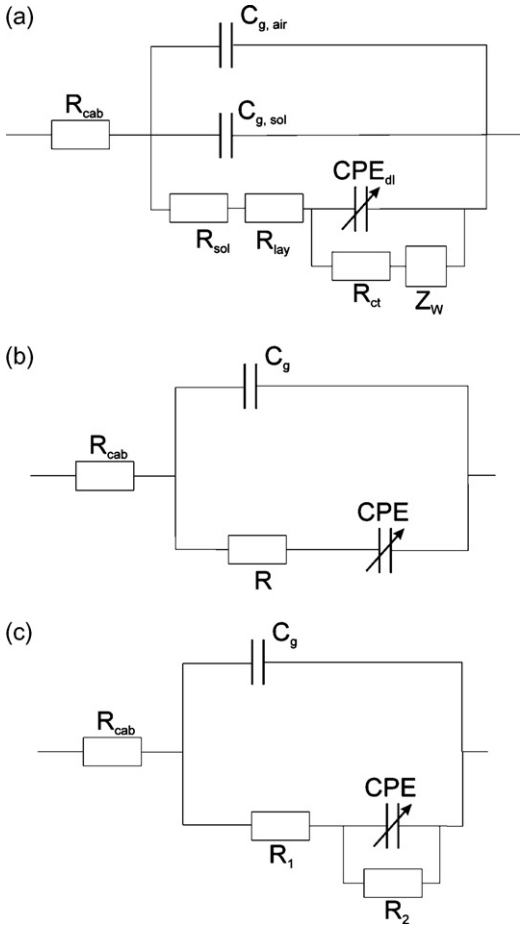

Fig. 5. Equivalent circuits. (a) Full EC to explain impedance between two electrodes partially immersed in a sol for EPD. R represents resistances of cables (cab), the sol between the two electrodes (sol), a deposited green layer (lay), R_{ct} the charge transfer resistance of an electrochemical reaction taking place, C_g the geometric capacitances between the electrode parts in air and in the sol. CPE_{dl} is a constant phase element representing the double layer capacitance of the electrodes, and Z_W is a Warburg impedance. Mathematically Z_W can also be described by a CPE in some cases. (b) Simplified EC to fit the impedance spectra between two Au electrodes in the absence of a deposited layer. (c) Simplified EC to fit the impedance spectra between a GC electrode and Au counter electrodes in the presence and absence of a green layer on the GC substrate.

series with a diffusional impedance, the Warburg impedance Z_W, the other one a constant phase angle element[1] CPE_{dl} describing the double layer capacitance.[33] This interfacial impedance corresponds to the typical modified Randles circuit widely applied in electrochemistry.[32,34] This EC still is a simplification, because in a more strict sense one would have to place two of these interfacial impedances in series, one for each Au electrode. In the case of the data shown in Fig. 1, R_{ct} was neglected because no electrochemical reactions were expected to take place under these conditions at open circuit potential, and therefore the simplified EC shown in Fig. 5b was used for data analysis. For the measurements between deposit-free GC and two Au electrodes $C_{g,air}$ could be omitted, since the GC substrate is fully immersed in the sol. However, now R_{ct} had to be considered (Fig. 5c), and the fit obtained with the equivalent circuit was not always satisfactorily, because the two interfaces (GC and Au) were different. In fact, a full description would contain three interfacial impedances, two in parallel (Au), one in series (GC), and also consider the geometry of the experimental arrangement. However, this was not necessary for the purpose of this work.

The impedance spectra after EPD looked similar and therefore were described with the same EC. Diffusion impedances were neglected in the current treatment (however, see discussion below).

4.2. Sol properties

Resistivity R and capacitance C_g obtained by fitting to the EC shown in Fig. 5b for the measurements in the sol are expected to obey the following relations:

$$R = \sigma^{-1}\frac{d}{A_{im}} + R_0 \quad (1)$$

$$C_g = C_0 + \varepsilon_0(A_{air} + \varepsilon_r A_{im})\frac{1}{d} \quad (2)$$

In these equations σ and ε_r represent the specific conductivity and the relative dielectric constant of the sol, respectively, and R_0 and C_0 account for non-zero intercepts. The other symbols have the same meaning as explained above.

R indeed depends linearly on the electrode distance (Fig. 6). From the linear fit one obtains $\sigma = 4.1 \times 10^{-5} \pm 8 \times 10^{-7}\,\mathrm{S\,cm^{-1}}$ and $R_0 = 6300\,\Omega$. This value for σ is larger than the number obtained by the Zetasizer measurements, but of the same order of magnitude. The differences might be caused by additional water uptake of the sol during the experiments in the EPD cell, which was open to the air. C scaled approximately linear with d^{-1} if one neglects the values for the largest and the smallest d. C_0 is rather large, 27 pF, and caused by the experimental arrangement (cables and connectors). This contribution also explains the large capacitance measured in air, that cannot be explained by the capacitance of two capacitor plates. From the slope of the linear fit ($2.2 \times 10^{-11} \pm 1 \times 10^{-12}\,\mathrm{F\,cm}$) one obtains $\varepsilon_r = 50.5 \pm 3$.

[1] $Z_{CPE} = Y_0^{-1}(j\omega)^{-\alpha}$, for $\alpha = 1$ equivalent to an ideal capacitance, for $\alpha = 0.5$ to a Warburg impedance, and for $\alpha = 0$ to a resistor.

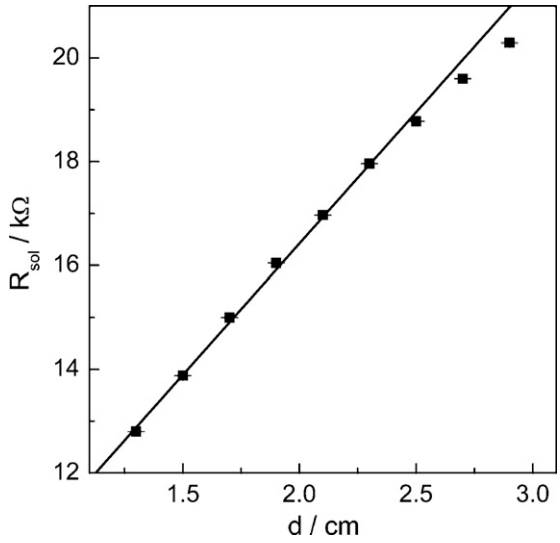

Fig. 6. Fit result for R_{sol} as a function of electrode distance d. The linear fit (neglecting the two values at largest d) is given by $R_{sol} = (6300 \pm 200)\,\Omega + (5060 \pm 100)\,\Omega\,\mathrm{cm^{-1}}\,d$.

This is much larger than the value for pure isopropanole, which is 20.18,[35] and also larger than values found for a powder-based YSI suspension. This might be in part due to the addition of nitric acid to the sol and some water uptake.

The origin of R_0 and the nature of the linear section shown in Fig. 1 are not fully clear. R_0 cannot be related to ohmic contributions of the cables or the Au-coated glass electrodes because in 0.5 M NaCl with the same setup resistances of less than 6 Ω were obtained. R_0 could be due to an interfacial contribution of an electroactive species (i.e. R_{ct} in Fig. 5a), that would not be dependent on electrode distance. However, this could only be true if the corresponding double layer capacitance C_{dl} was of similar order of magnitude as C_g. Otherwise the fit and the data would not match. This in turn is six orders of magnitude less than typical values for C_{dl}, and therefore very low even considering the low ionic concentrations and the organic solvent. Additionally, the value of R_0 is too low given the absence of significant amounts of electroactive species in the sol. Therefore R_0 is not a charge transfer resistance. The linear region of the impedance spectra at low frequencies (cf. Fig. 1) could be due to the double layer capacitance or to a diffusional impedance. The exponents of the fits with a constant phase element are approximately 0.67, and therefore larger than expected for a Warburg impedance (0.5), but smaller than expected for a double layer capacitance at smooth electrodes (close to 1). However, if one plots for the spectra from Fig. 1 1/Im(Z) for low frequencies versus ω one obtains straight lines and from the slope one can estimate C_{dl} as 12–18 $\mu\mathrm{F\,cm^{-2}}$, without any clear dependence on the electrode distance. These values are large given the small ionic strength of the sol, but of the correct order of magnitude. A fit with a Warburg impedance, on the other hand, would require a concentration of an electroactive species of about 10 $\mu\mathrm{mol\,l^{-1}}$ assuming a diffusion coefficient of $10^{-6}\,\mathrm{cm^2\,s^{-1}}$. Therefore the interpretation of the line at low frequencies as double layer capacitance in the absence of any faradaic reaction seems to be more reasonable.

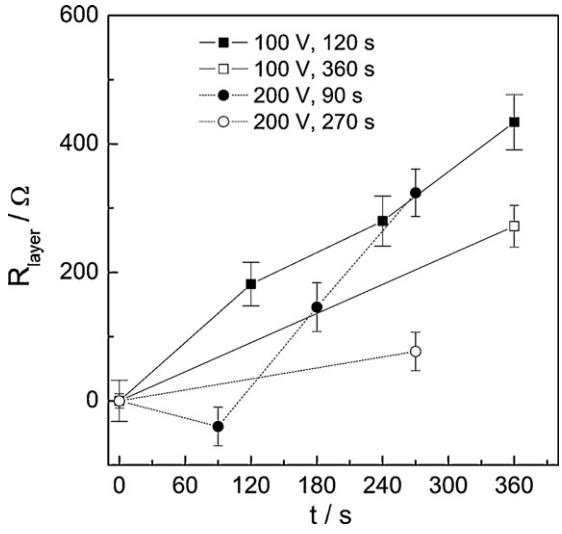

Fig. 7. Resistance of green layers obtained from impedance measurements after stepwise and one-step depositions.

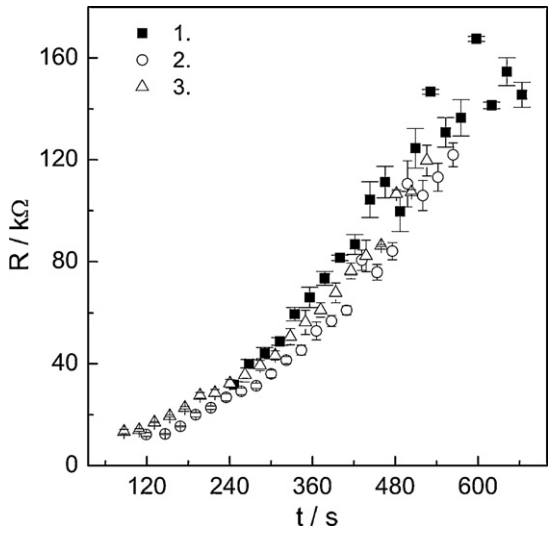

Fig. 8. Changes in charge transfer resistance with time after the end of each of three consecutive EPD steps (100 V, 120 s).

4.3. Impedance in the presence of a deposit

The presence of the deposit did not alter the impedance behavior significantly. It was still mainly controlled by the properties of the sol. The slight curvature of the low frequency part before EPD was probably caused by the substrate geometry and small asymmetries in the experimental setup. The equivalent circuit in Fig. 5c described the data satisfactorily. The most important change in the impedance spectra during stepwise deposition was a small increase in the values found for $R_{sol} + R_{lay}$ (Fig. 7), that can explain that the first current measured in a deposition experiment after a break was somewhat less than in the beginning of the first deposition (Fig. 2). The amount of increase in R_{lay} scattered from experiment to experiment, and did not show a clear dependence of the applied voltage. This is very different compared to deposition from a powder-based Y_2SiO_5 suspension,[26] where an increase in deposition time and in deposition voltage caused a reproducible increase in R_{lay}. In both cases, however, the increases in R_{lay} were much less than the resistance of the sol itself, and therefore did not contribute to explain the current transients during EPD (Fig. 2). However, Stappers et al. showed performing impedance measurements at 1 kHz during EPD from alumina suspensions that the resistance of the layer measured during EPD was much larger than after turning off the external field.[22]

This is supported in this work by the rapid changes in impedance response after turning off the deposition voltage, as described above (cf. Section 3.2 and Fig. 4), both at low and especially at high frequencies. From fits with simplified equivalent circuits the corresponding resistances were extracted (Figs. 8 and 9). The resistance at low frequencies (R_2 in Fig. 5c, Fig. 8), which is in parallel to the double layer capacitance, can be considered as a charge transfer resistance. It clearly increased with time after the end of deposition. At the same time the corresponding double layer capacitance also increased to some extent. The behavior after the first and following deposition steps was very similar, indicating that the thickness of the deposit had not as big an impact as might have been expected from Fig. 3.

The resistance at high frequencies decreased with time (Fig. 9, R_1 from Fig. 5c, equals sum of R_{sol} and R_{lay} from Fig. 5a). This decrease was associated with a decrease in the layer resistivity. This is consistent with the rapid drop in R_{lay} reported in literature after turning off the deposition.[22] There are a number of explanations in literature to explain the potential drop over the deposit layer causing transients like the ones in Fig. 2 (see also Section 1). Anné et al. suggested that if the Debye length is of the same order of magnitude as the pore diameters the corresponding potential covers the entire diameter of the pore and impedes ionic mass transport.[24] This model was in contradiction to experimental findings and calculations by Stappers et al.[22] De and Nicholson suggested that the consumption of H^+ in acidic suspensions will cause the formation of an ion depleted layer at the electrode.[25] This idea was further elaborated by van Tassel et

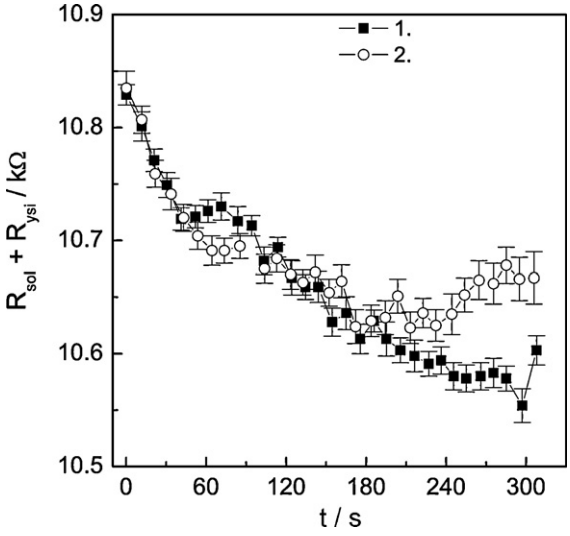

Fig. 9. Changes in sol and EPD layer resistance with time after the end of each of two consecutive EPD steps (100 V, 120 s).

al for HCl containing suspensions, where in addition to the consumption of H^+ the rapid migration of counter ions away from the cathode was postulated, leading to a severely ion depleted layer close to the electrode, which is stabilized by the deposit.[23] Such an ion depleted layer would cause high resistances during deposition, and after turning off the voltage, diffusion of H^+ and Cl^- (or nitrate in this work) from suspension would cause it to decrease again rapidly. This model was consistent with the findings of Stappers, and could also explain the change of R_{lay} seen in this work (Fig. 9). It could not explain the low values of R_{ct} immediately after the end of deposition (Fig. 8).

The latter could be explained by an influence of the electrode reaction product formed during EPD. The charge carriers for electrical current flux through the sol are the yttrium silicate particles and dissolved ions, mainly protons, potassium ions and nitrate ions. While the deposition voltage is turned on, at the negative electrode a porous, solvent-rich layer forms due to EPD. In parallel electrochemical reactions take place at the interface between substrate/sol (beginning of deposition) or substrate/layer (deposit present) in order to supply the electrons flowing in the outer circuit. In the isopropanol solution containing some water and nitric acid as well as the positively charged YSI particles the most probable cathodic electrode reaction is hydrogen evolution,[15,24,25] leaving behind nitrate ions, and, depending on local pH, possibly hydroxyl ions (from dissolved water) and of course the deposit. Nitrate ions migrate out of the deposit for sake of charge balance and due to the applied field. After turning off the externally applied deposition voltage, deposition stops, and the hydrogen present in the layer forms (together with protons or water) a reversible redox couple, that controls the open circuit potential of the electrode and provides a low charge transfer resistance (R_2 in Fig. 5c). If this hydrogen partially blocks pores in the deposit and parts of the surface, then it contributes to the higher resistance of the deposit (R_1 in Fig. 5c). With time, hydrogen diffuses out of the pores, causing an increase in R_{ct}, an increase in the accessible electrode area and thus C_{dl}, and possibly a decrease of pore clogging and therefore in R_{lay}. Such effects can also have an impact on the deposition process itself.

4.4. Electrophoretic deposition process

The mechanisms involved even in the formation of electrophoretic deposits from simple powder suspensions are not fully understood. This concerns also the role of the electrode reactions involved in the EPD process and the explanation of the kinetics. The situation is even more complicated in the case of EPD from a sol containing a number of ionic species and particles with a possibly different surface chemistry as compared to dispersed oxide particles. This study clearly confirms that electrophoretic deposition of ceramic materials from a polymeric precursor sol is possible, and that impedance spectroscopy can help to provide some insight in the processes involved. Of the different explanations provided in literature for the decay of current during potentiostatic deposition (Fig. 2) the role of a resistance of the layers caused by the solid volume content as the major culprit was not supported. However, results were in agreement with ion depletion within the film during EPD, even though no direct proof can be obtained from these measurements. The formation of hydrogen, however, could have some influence as well as the rate of outward diffusion of reaction products (nitrate ions, hydrogen, hydroxyl ions) and the inward transport of charge carriers (protons) towards the electrode. These transport processes will become more and more difficult with increasing layer thickness. The data presented here delivered some evidence for the role of electroactive intermediates during EPD. Evidence for diffusion-controlled processes was seen in the time dependence of the current transients at longer deposition times. With increasing deposit thickness the hydrogen formed needs more time to diffuse out of the layer, and the solvent and protons more time to reach the surface (even though proton transport might be accelerated due to the increasing field strength across the deposit). In order to obtain direct evidence for transport control from impedance data and to probe the existence of a ion depletion layer for EPD from the polymeric precursor sol it would be necessary to perform IS measurements in the presence of an applied electric field, similar to procedures in earlier work[26] and in literature.[22]

In the very beginning the EPD currents correlated very well with the resistance of the sol ($+R_0$). This indicates that electrochemical reactions are taking place fast. During the early stages of EPD apparently no deposit was formed at all, even though the formation of a monolayer cannot be excluded. Therefore the current changes there could be related to electrochemical reactions (hydrogen evolution) and formation of concentration/pH gradients as well as reactions between the particles, before the formation of the deposit influences the further kinetics. Such delays were explained in literature by a need for an increase in electrolyte[15] or particle concentration[16] or in pH[25] to induce flocculation. The overall amount deposited was much less than typically obtained from powder-based suspensions, even though much higher voltages were applied. In addition there was no clear correlation between deposition conditions (time, charge, voltage) and mass. Obviously the deposition mechanism from polymeric precursor sols is more complicated than from powder deposits, and sensitive regarding the exact chemical composition and therefore the zetapotential and mobility of the particles. However, the deposition from these precursor sols led to the correct chemical composition of the green layer, and offers a larger versatility in comparison to powder dispersions.

5. Conclusions

A polymeric precursor sol allowed the EPD of yttrium silicate under varying experimental conditions. Similar to powder-based suspensions the current transients showed a rapid decrease in current and therefore in deposition rate. However, the relation between the preparation conditions and the obtained amounts of deposit were not as well defined for the employed sol composition and the applied deposition conditions. Nevertheless this method opens new prospects for the formation of ceramic coatings by EPD. Impedance spectroscopy allowed to characterize the properties of the sol before the deposition experiments, and pointed to an important role of electrochemical reaction prod-

ucts to the deposition kinetics, indicated by a rapid change in the resistance of the green body and the charge transfer resistance, that determined the diameter of the low frequency semicircle in the impedance spectra. In addition a contribution of mass transport processes through the deposited layers is possible. In order to completely understand the EPD kinetics and check for the influence of the deposit resistance during EPD IS measurements in presence of an applied electric field are required.

Acknowledgement

Financial support from the Deutsche Forschungsgemeinschaft (DFG) is gratefully acknowledged.

References

1. Buckley, J. D., Carbon–carbon overview in carbon–carbon materials and composites. *NASA Reference Publication*, 1992, **1254**, 1.
2. De Castro, L. D. and McEnaney, B., The control of high temperature corrosion of engineering carbons and graphites. *Corrosion Science*, 1992, **33**, 527–543.
3. Luthra, K. L., Oxidation of carbon/carbon composites—a theoretical analysis. *Carbon*, 1988, **26**, 217–224.
4. Buchanan, F. J. and Little, J. A., Glass sealants for carbon–carbon composites. *Journal of Material Science*, 1993, **28**, 2324–2330.
5. Morimoto, T., Ogura, Y., Kondo, M. and Ueda, T., Multilayer coating for carbon–carbon composites. *Carbon*, 1995, **33**, 351–357.
6. Ogura, Y., Kondo, M., Morimoto, T., Notomi, A. and Sekigawa, T., Oxygen permeability of Y_2SiO_5. *Materials Transactions*, 2001, **42**, 1124–1130.
7. Aparicio, M. and Duran, A., Yttrium silicate coatings for oxidation protection of carbon–silicon carbide composites. *Journal of the American Ceramic Society*, 2000, **83**, 1351–1355.
8. Huang, J.-F., Li, H.-J., Zeng, X.-R., Li, K.-Z., Xiong, X.-B., Huang, M. *et al.*, A new SiC/yttrium silicate/glass multi-layer oxidation protective coating for carbon/carbon composites. *Carbon*, 2004, **42**, 2356–2359.
9. Argirusis, C., Damjanović, T., Stojanović, M. and Borchardt, G., Yttrium silicate coating system for oxidation protection of C/C–Si–SiC composites: electrophoretic deposition and oxygen self-diffusion measurements. *Journal of the European Ceramic Society*, 2007, **27**, 1303–1306.
10. Trusty, P. A., Ponton, C. B. and Boccaccini, A. R., Fabrication of woven nicalon (NL607) SiC fibre–yttrium disilicate CMCs using electrophoretic deposition. *Ceramic Transactions*, 1998, **83**, 391–398.
11. Damjanović, T., Argirusis, C., Borchardt, G., Leipner, H., Herbig, R., Tomandl, G. *et al.*, Oxidation protection of C/C–SiC composites by an electrophoretically deposited mullite precursor. *Journal of the European Ceramic Society*, 2005, **25**, 577–587.
12. Castro, Y., Ferrari, B., Moreno, R. and Duran, A., Electrophoretic deposition (EPD) coatings of sol–gel solutions and suspensions. *Journal of Sol–Gel Science and Technology*, 2002, **23**, 187–189.
13. Grosse-Brauckmann, J., Borchardt, G. and Argirusis, C., Preparation and electrophoretic deposition of an yttrium silicate precursor sol. *Key Engineering Materials*, 2009, **412**, 267–272.
14. Besra, L. and Liu, M., A review on fundamentals and applications of electrophoretic deposition (EPD). *Progress in Materials Science*, 2007, **52**, 1–61.
15. Fukada, Y., Nagarajan, N., Mekky, W., Bao, Y., Kim, H.-S. and Nicholson, P. S., Electrophoretic deposition—mechanisms, myths and materials. *Journal of Materials Science*, 2004, **39**, 787–801.
16. Sarkar, P. and Nicholson, P. S., Electrophoretic deposition (EPD): mechanism, kinetics and application to ceramics. *Journal of the American Ceramic Society*, 1996, **79**, 1987–2002.
17. Zhitomirsky, I., Cathodic electrodeposition of ceramic and organoceramic materials; fundamental aspects. *Advances in Colloid and Interface Science*, 2002, **97**, 279–317.
18. Corni, I., Ryan, M. P. and Boccaccini, A. R., Electrophoretic deposition: from traditional ceramics to nanotechnology. *Journal of the European Ceramic Society*, 2008, **28**, 1353–1367.
19. Anné, G., Vanmeensel, K., Vleugels, J. and van der Biest, O., A mathematical description of the kinetics of the electrophoretic deposition process for Al_2O_3-based suspensions. *Journal of the American Ceramic Society*, 2005, **88**, 2036–2039.
20. Kershner, R. J., Bullard, J. W. and Cima, M. J., The role of electrochemical reactions during electrophoretic particle deposition. *Journal of Colloid and Interface Science*, 2004, **278**, 146–154.
21. Koura, N., Tsukamoto, T., Shoji, H. and Hotta, T., Preparation of various oxide films by an electrophoretic deposition method: a study of the mechanism. *Japanese Journal of Applied Physics*, 1995, **34**, 1643–1647.
22. Stappers, L., Zhang, L., van der Biest, O. and Fransaer, J., The effect of electrolyte conductivity on electrophoretic deposition. *Journal of Colloid and Interface Science*, 2008, **328**, 436–446.
23. van Tassel, J. J. and Randall, C. A., Role of ion depletion in the electrophoretic deposition of alumina powder from ethanol with increasing quantities of HCl. *Journal of Materials Science*, 2006, **41**, 8031–8046.
24. Anné, G., Neirinck, B., Vanmeensel, K., van der Biest, O. and Vleugels, J., Origin of the potential drop over the deposit during electrophoretic deposition. *Journal of the American Ceramic Society*, 2006, **89**, 823–828.
25. De, D. and Nicholson, P. S., Role of ionic depletion in deposition during electrophoretic deposition. *Journal of the American Ceramic Society*, 1999, **82**, 3031–3036.
26. Argirusis, C., Damjanović, T. and Schneider, O., An impedance study of the electrophoretic deposition from yttrium silicate suspensions. *Journal of Materials Science*, 2006, **41**, 8059–8067.
27. Anné, G., Vanmeensel, K., Vleugels, J. and van der Biest, O., Influence of the suspension composition on the electric field and deposition rate during electrophoretic deposition. *Colloids and Surfaces A: Physicochemical and Engineering Aspects*, 2004, **245**, 35–39.
28. Zhang, Z., Huang, Y. and Jiang, Z., Electrophoretic deposition forming of SiC–TZP composites in a nonaqueous sol media. *Journal of the American Ceramic Society*, 1994, **77**, 1946–1949.
29. Biesheuvel, P. M. and Verweij, H., Theory of cast formation in electrophoretic deposition. *Journal of the American Ceramic Society*, 1999, **82**, 1451–1455.
30. Negishi, H., Yamaji, K., Imura, T., Kitamoto, D., Ikegami, T. and Yanagishita, H., Electrophoretic deposition mechanism of YSZ/n-propanol suspension. *Journal of The Electrochemical Society*, 2005, **152**, J16–J22.
31. Bard, A. J. and Faulkner, L. R., *Electrochemical Methods: Fundamentals and Applications* (*2nd ed.*). John Wiley & Sons, New York, 2001.
32. Macdonald, J. R., *Impedance Spectroscopy—Emphasizing Solid Materials and Systems*. John Wiley & Sons, New York, 1987.
33. Cole, K. S. and Cole, R. H., Dispersion and absorption in dielectrics. I. Alternating current characteristics. *Journal of Chemical Physics*, 1941, **9**, 341–351.
34. Randles, J. E. B., Kinetics of rapid electrode reactions. *Faraday Society Discussions*, 1947, **1**, 11–19.
35. Linde, D. R., ed., *CRC Handbook of Chemistry and Physics*. 83rd ed. CRC Press, Boca Raton, London, New York, Washington, 2002, pp. 6–157.